Solid State Sciences 14 (2012) 1282–1288

Contents lists available at SciVerse ScienceDirect

Solid State Sciences

journal homepage: www.elsevier.com/locate/ssscie

Characteristics of SnO_2 thin films prepared by SILAR

M. Ali Yıldırım [a,*], Yunus Akaltun [b], Aytunç Ateş [c]

[a] Department of Physics, Science and Art Faculty, Erzincan University, 24030 Erzincan, Turkey
[b] Department of Electrical and Electronic, Engineering Faculty, Erzincan University, Erzincan, Turkey
[c] Department of Material Engineering, Engineering and Natural Sciences Faculty, Yıldırım Beyazıt University, Ankara, Turkey

ARTICLE INFO

Article history:
Received 19 March 2012
Received in revised form
6 June 2012
Accepted 10 July 2012
Available online 20 July 2012

Keywords:
SnO_2
Film thickness
Refractive index
Dielectric constant
SILAR

ABSTRACT

SnO_2 thin films were deposited on glass substrates by using Successive Ionic Layer Adsorption and Reaction (SILAR) method at room temperature. The film thickness effect on characteristic parameters such as structural, morphological, optical and electrical properties of the films was studied. Also, the films were annealed in oxygen atmosphere (400 °C, 30 min) and characteristic parameters of the films were investigated. The X-ray Diffraction (XRD) and Scanning Electron Microscopy (SEM) studies showed that all the films exhibited polycrystalline nature with tetragonal structure and were covered well on glass substrates. After the investigation of the crystalline and surface properties of the films, it was found that they were improving with increasing film thickness. **Optical band gap decreased from 3.90 eV to 3.54 eV and electrical conductivity changed between 0.015–0.815 $(\Omega\text{-cm})^{-1}$ as the film thickness increased from 215 to 490 nm.** The refractive index (n), optical static and high frequency dielectric constants (ε_0, ε_∞) values were calculated by using the optical band gap values as a function of the film thickness.

© 2012 Published by Elsevier Masson SAS.

1. Introduction

Transparent Conducting Oxides (TCOs), such as tin oxide, zinc oxide, cadmium oxide, indium oxide, etc have been widely studied for their use in optoelectronic device and solar energy technology. Due to their optical and electrical properties, TCOs are used for photovoltaic solar cells, phototransistors, liquid crystal display, optical heaters, gas sensors, transparent electrodes and other optoelectronic devices [1,2]. Of these TCOs, tin oxide (SnO_2) has attracted most attention for various applications such as solar cells, gas sensors, transparent electrodes in display devices like liquid crystal displays, infrared reflectors, plasma display panels, transistors, etc. [3–6]. Among the semiconducting metal oxides used for gas sensors, SnO_2 is the most widely used material due to its low cost, long-life and good reproducibility. SnO_2 sensors are used for various purposes, such as detecting inflammable and harmful gases like hydrogen (H_2), carbon monoxide (CO) and nitrous oxide (NO_x) compounds [6,7].

SnO_2 is n-type semiconducting oxide with wide band gap ($E_g = 3.6$ eV at 300 K) and is grown as tetragonal crystal structures [5,8]. SnO_2 thin films have low resistivity and high optical transparency in the visible region of electromagnetic spectrum. This high transparency is caused by wide bandgap of these films. The electrical properties of SnO_2 thin films depend on oxygen vacancies, doping concentration, film thickness, microstructure, deposition conditions such as deposition temperature, substrate temperature, precursor solutions, etc [3,6,9,10]. In addition, SnO_2 is useful as a hard film material for applications requiring high refractive and reflective properties [11,12].

SnO_2 thin films have some advantage in contrast to other TCO films that contain expensive, scarcity and toxic elements (In, Ti, Cd etc.). SnO_2 has better thermal resistance than indium tin oxide (ITO), its films are relatively hard and they have good abrasion and scratch resistance [13]. High hardness of SnO_2 films is important for application of transparent conductive films as protective layers on soft and transparent substrates, such as polymer materials for vehicular and aircraft canopies, windows and windshields [14]. Thus, the properties of SnO_2 and its relatively low cost, make it preferable in some applications requiring a conducting layer on glass.

SnO_2 thin films have been prepared by various methods such as electron beam evaporation [3], pulsed laser deposition [4], chemical vapor deposition [15], spray pyrolysis [6,9], SILAR [5]. Among these, SILAR is simple, cost effective and reproducible. It is a unique method by which thin films of compound semiconductors can be deposited alternately by means of the dipping substrate into the aqueous solutions of containing ions for each component. Also, different oxide films such as ZnO [2], $CdO/Cd(OH)_2$ [16] have been

* Corresponding author. Tel.: +90 446 2243097; fax: +90 446 2243016.
E-mail address: mayildirim@erzincan.edu.tr (M.A. Yıldırım).

1293-2558/$ – see front matter © 2012 Published by Elsevier Masson SAS.
http://dx.doi.org/10.1016/j.solidstatesciences.2012.07.012

prepared by SILAR method. These studies have shown that SILAR is suitable method to prepare TCO thin films.

In this paper, SnO_2 thin films have been deposited on glass substrates using SILAR method. The film thickness and annealing effects on the structural, morphological, optical and electrical properties of SnO_2 thin films have been investigated. Also, for fabrication and simulation of SnO_2 based devices, accurate determination of some parameters such as refractive index and dielectric constants is an essential prerequisite. We focus film thickness effect on refractive index (n), static and high frequency dielectric constants (ε_0, ε_∞). Characterization of the films has been done using XRD, SEM, optical absorption measurements and the two-point-probe method.

2. Experimental procedure

In this study, SnO_2 thin films were deposited on glass substrates using SILAR method at room temperature and ambient pressure. To deposit SnO_2 thin films, aqueous tin–ammonia complex ions ($[Sn(NH_3)_4]^{4+}$) were chosen for the cation precursor, in which analytical reagents of $SnCl_4$ (%99) and concentrated ammonia 0.8 M $NH_{3(aq)}$ (25–28%) were used. The concentration values defined for the tin (Sn) solution was 0.1 M and the molar ratio of Sn:NH_3 is 1:8 obtained for SnO_2 thin films as a result of several experiments.

Substrate cleaning plays an important role in the deposition of thin films. The glass substrates were cleaned ultrasonically for 10 min, first in acetone and then in a 1:1 ethanol: water solution. The substrates were dried and stored in desiccators.

To deposit SnO_2 thin films, one SILAR growth cycle involves the four following steps: 1) immersing the substrate in the precursor solution for 20 s to create a thin liquid film containing $[Sn(NH_3)_4]^{4+}$on the substrate; 2) immersing immediately the withdrawn substrates in hot water (90 °C) for 7 s to form a SnO_2 layer; 3) drying the substrate in the air for 60 s and 4) rinsing the substrate in a separate beaker for 40 s to remove large and loosely bonded SnO_2 particles. Thus one SILAR cycle of SnO_2 deposition was completed. The adsorption, reaction and rinsing times were chosen experimentally so that deposition occurred layerwise and resulted in homogeneous thin film structure. The film thickness has been defined as 215, 300, 380 and 490 nm by repeating 60, 80, 100 and 120 SILAR growth cycle, respectively.

To investigate the film thickness effect on the characteristic parameters of the films, XRD, SEM, optical absorption measurements and the two-point-probe method were used. Also, the films were annealed in oxygen atmosphere (400 °C, 30 min) and characteristic parameters of the films were investigated. For structural studies, a Rigaku 2200D/Max, X-Ray Diffractometer using Cu Kα (λ = 1.5405 Angstrom (Å)) radiation with 2θ of 20-60° was used. Surface morphology was studied using the Zeiss Supra 50 VP model SEM. In order to study the optical properties of the generated films, the absorption measurements were carried out using a Perkin–Elmer UV/VS Lambda 2S Spectrometer with a wavelength resolution better than ±0.3 nm at room temperature. As the films were examined along with the substrates on which they were formed, it was necessary to take into account the absorbance in the glass substrate even though it was small. Hence, the absorbance spectra of the glass substrates were taken and used for the elimination of the optical absorbance in the glass substrate from the total absorbance in the film–substrate combination to obtain the optical absorbance of the film. The electrical conductivity of these films was measured using the two-point-probe method in the temperature range of 300–500 K. Silver (Ag) dots with diameter of about 1.0 mm were evaporated on the films by thermal resistive heating technique and the contact area was obtained as 7.85×10^{-3} cm^{-2}. All evaporation processes were carried out in a turbo molecular vacuum coating unit at about 10^{-5} torr.

3. Result and discussion

3.1. Structural analysis

The structural analysis of SnO_2 thin films was carried out by using XRD varying the diffraction angle, 2θ from 20 to 60°. The XRD patterns of the films are shown in Figs. 1 and 2. The XRD patterns of the films indicate the existence of a SnO_2 single phase with a tetragonal structure [3,5]. As seen in Fig. 1, all the films have polycrystalline structure with orientation along with different planes. These planes are (110), (101), (200), (210), (211), (220) and (002). It was observed that all the films have the same crystal structure but the intensities and full width at half maximum (FWHM) values of these peaks change with different film thickness. While the diffraction peak intensities increase, half maximum values of these peaks decrease with increasing film thickness. These changes may be attributed to the improvement of crystallinity of the films and removal of the defects with increasing the film thickness. It is seen in Fig. 1, although some peaks appear and some peaks disappear with changing film thickness, the (110) peak is still dominant peak in all the films. The best crystallinity was seen in 380 nm film thickness. It was found for all films that, the crystallinity begins to break down after 380 nm film thickness. As is seen in Fig. 2, film crystallinity is improved with annealing temperature (400 °C). The broad hump in the range $2\theta = 20–35°$ is due to the amorphous glass substrate. All of these results are in agreement with relevant literature [2,4,5,9].

The texture coefficient (TC) represents the texture of a particular plane, deviation of which from unity implies the preferred growth. Quantitative information concerning the preferential crystallite orientation was obtained from different texture coefficient TC(hkl) defined by well–known relation [17],

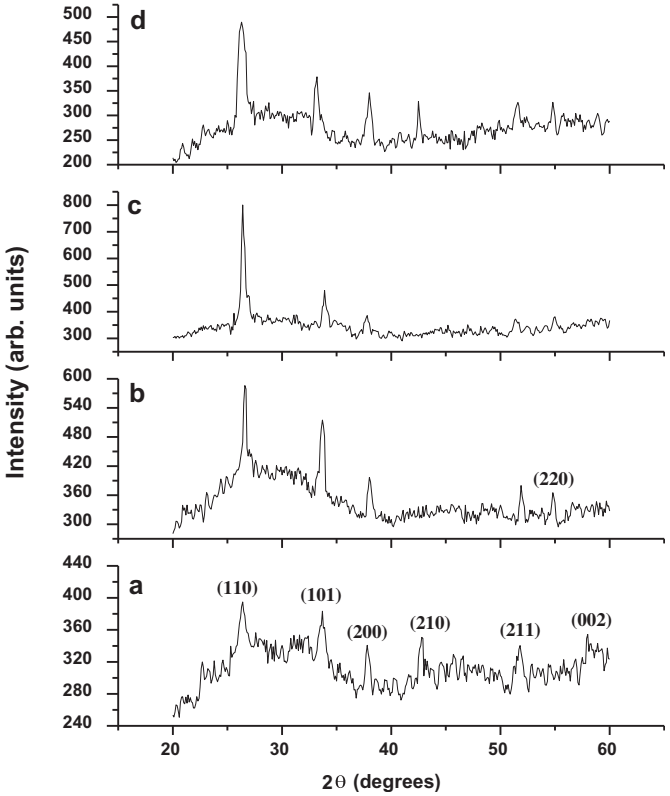


Fig. 1. The XRD patterns of SnO_2 thin films [(a) 215 nm, (b) 300 nm, (c) 380 nm, (d) 490 nm].

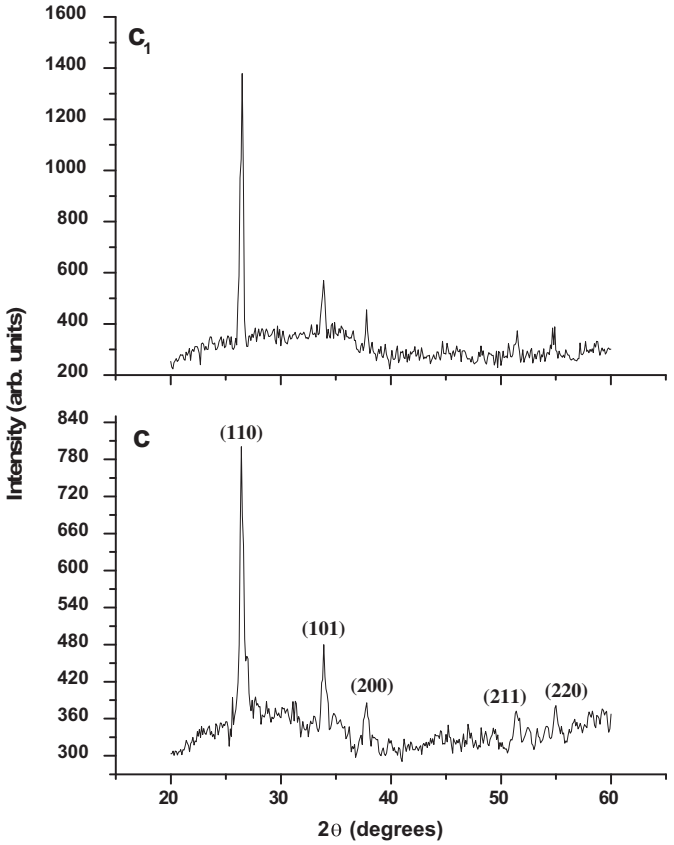


Fig. 2. The XRD patterns of (c) as-Deposited and (c_1) annealed SnO_2 thin films in O_2 atmosphere for 30 min at 400 °C.

$$TC(hkl) = \frac{I(hkl)/I_0(hkl)}{N^{-1}\sum_n I(hkl)/I_0(hkl)} \quad (1)$$

where I(h k l) is the measured relative intensity of a plane (h k l), I_0(h k l) is the standard intensity of the plane (h k l) taken from the JCPDS data, N is the reflection number and n is the number of diffraction peaks. A sample with randomly oriented crystallite presents TC(hkl) = 1, while the larger this value, the larger abundance of crystallites oriented at the (h k l) direction. The texture coefficients were calculated for all diffraction peaks and were given in Table 1. As is seen from Table 1, the highest TC is in (110) plane for all the films.

The structural parameters such as grain size (D), dislocation density (δ), FWHM (β), strain (s) for all films were evaluated by XRD patterns. The grain size of the thin films was calculated by XRD patterns using Debye Scherrer's formula,

Table 1
TC (hkl) values of SnO_2 thin films as a function of film thickness and annealed temperature.

(hkl)	SnO_2 (215 nm)	SnO_2 (300 nm)	SnO_2 (380 nm)	SnO_2 (490 nm)	SnO_2 (380 nm) annealed 400 °C
	TC (hkl)	TC (hkl)	TC (hkl)	TC (hkl)	TC (hkl)
(110)	1.405	1.779	2.127	1.546	2.427
(101)	1.292	1.174	1.191	1.082	0.946
(200)	0.772	0.782	0.595	0.897	0.679
(210)	0.871	–	–	0.850	–
(211)	0.758	0.693	0.531	0.804	0.461
(220)	–	0.569	0.553	0.819	0.485
(002)	0.899	–	–	–	–

$$D = \frac{0.9\lambda}{\beta \cos\theta} \quad (2)$$

where D is the grain size, λ is the used X-Ray wavelength, β is the angular line width at half-maximum intensity in radians and θ is Bragg's angle. The grain size, dislocation density and strain of the films were calculated using the FWHM for (110) peak. Additionally, to have more information on the amount of defects in the films, the dislocation density (δ) was calculated by using the formula below [2,18],

$$\delta = \frac{1}{D^2} \quad (3)$$

The strain values were calculated from the following relation [19],

$$s = \frac{\beta \cos\theta}{4} \quad (4)$$

While the grain size values increase from 6.63 nm to 19.92 nm, the dislocation density and strain values decrease from 227.22×10^{-4} nm^{-2} to 25.19×10^{-4} nm^{-2}and from 0.29 line^{-2} m^{-4} to 0.09 line^{-2} m^{-4} with increasing film thickness, respectively [4]. But these parameters exhibit opposite changing after 380 nm thickness. These changes may be attributed to the improving of the film crystallinity. Also, while the grain size value increases 24.01 nm, the dislocation density and strain values decrease 17.33×10^{-4} nm^{-2} and 0.08 line^{-2} m^{-4} with annealing temperature (400 °C), respectively. Larger D, smaller β, δ and s values indicate better crystallization of the films. For this study it can be said that, the better crystallization structure has been obtained for 380 nm film thickness and the annealing temperature plays important role on the characteristic parameters of the films accordance to the D, β, δ and ε values (Figs. 1 and 2 and Table 1).

3.2. Surface morphological analysis

It is known that the surface properties of the TCO films influence their optical and electrical properties which are important factors in applications of optoelectronic devices. For example, the increase in surface roughness of the films leads to an increase in the propagation loss for surface acoustic wave (SAW) devices and a decrease in the efficiency of photovoltaic solar cells. Therefore, it is very important to investigate the surface morphology of the films [2]. Fig. 3 shows the SEM images of as-deposited SnO_2 thin films for different film thickness. It is obvious from Fig. 3a that, the film does not have a smooth and homogeneous surface morphology with holes and cracks for 215 nm film thickness. The uniform, dense, smooth and well-adhered to the substrates of the films increased with increasing film thickness (Fig. 3b–c). For 490 nm thickness (Fig. 3d), the level of surface roughness increases while the film surface deteriorates. Fig. 4 shows the SEM images of as-deposited (380 nm) and annealed SnO_2 thin films. The annealed film surface is better and more compact, denser and more uniform compared the as-deposited film. The grains combined together to form crystalline film by annealing, thereby increasing the grain size. Consequently, the surface properties of the SnO_2 thin films significantly change with film thickness and annealing temperature [2,9]. Especially, for 380 nm thickness, all of the surface properties are better than the others. These results are in agreement with XRD measurements [2].

3.3. Optical characterization

Absorption measurements were carried out at room temperature. The optical band gaps of SnO_2 films were calculated by using

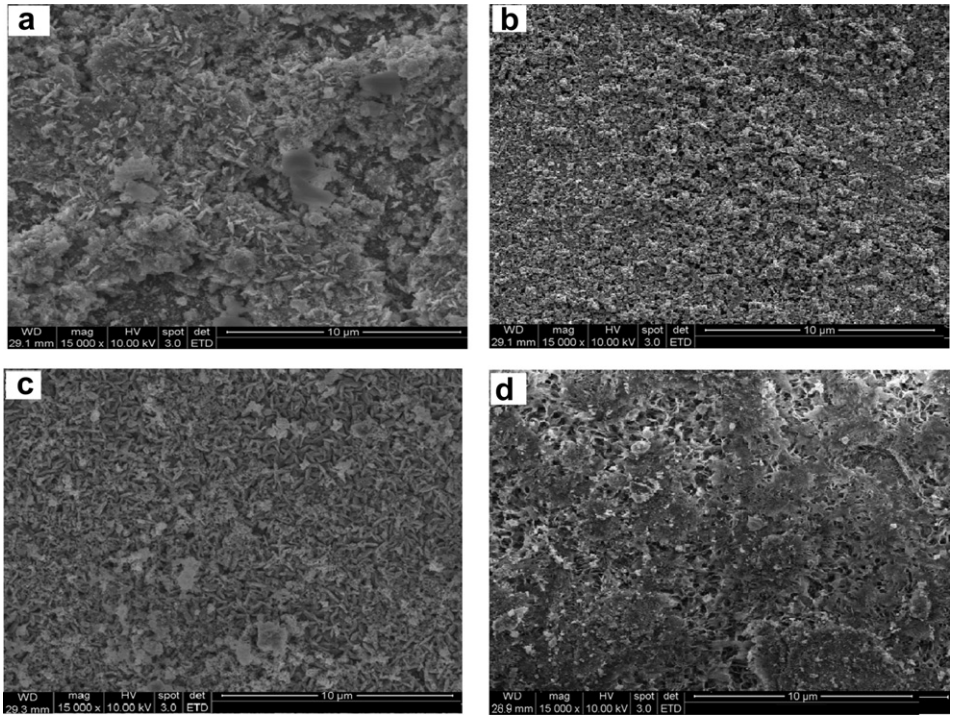


Fig. 3. SEM images of SnO_2 thin films [(a) 215 nm, (b) 300 nm, (c) 380 nm and (d) 490 nm] at 15000× magnification.

the optical absorption spectra. To determine the optical band gap values, we plotted $(\alpha h\nu)^2$ versus $(h\nu)$ where α is the absorption coefficient and $h\nu$ is the photon energy. The theory of interband absorption shows that at the edge of optical absorption the absorption coefficient α varies with the photon energy $h\nu$ according to the [2,20],

$$\alpha = \frac{A}{h\nu}(h\nu - E_g)^n \tag{5}$$

where A is a constant, E_g is the optical band gap and n assumes values of 1/2, 2, 3/2 and 3 for allowed direct, allowed indirect, forbidden direct and forbidden indirect transitions, respectively. The band gap energies of the films were determined by the extrapolation of the linear regions on the energy axis $(h\nu)$, as shown in Fig. 5.

The film thickness and annealing effects on the absorption measurements were investigated. As is seen from the Fig. 5 and Table 2, the band gap values decreased from 3.90 to 3.54 eV with increasing film thickness and from 3.74 for 380 nm film thickness to 3.66 eV with annealing temperature (400 °C), respectively. The decreasing in band gap with increasing film thickness can be attributed to the improvement in the crystallinity, morphological changes, changes of atomic distances and grain size. During the growth process some impurity (oxygen vacancies and/or Sn interstitials etc.) levels [6,21,22] take place near the conduction band with increasing film thickness [2]. There is a possibility of structural defects in the films due to their preparation conditions; this could give rise to the allowed states near the conduction band in the forbidden region. These allowed states may merge with the conduction band with increasing film thickness and resulting in the reduction of the band gap. Also, decreasing in band gap with annealing effect can be attributed to the improvement in the crystallinity and surface properties, removal of tin hydroxide accumulation along grain boundaries with annealing, which is more common phenomena in chemically deposited thin films. These results are in agreement with our XRD and SEM results and literature [2,5,22–24].

The refractive index (n) and dielectric constant (ε) of semiconducting materials is very important in determining the optical and electrical properties of the crystals. Knowledge of n is essential in the design of heterostructure lasers in optoelectronic devices as well as in solar cell applications. The refractive index of the films

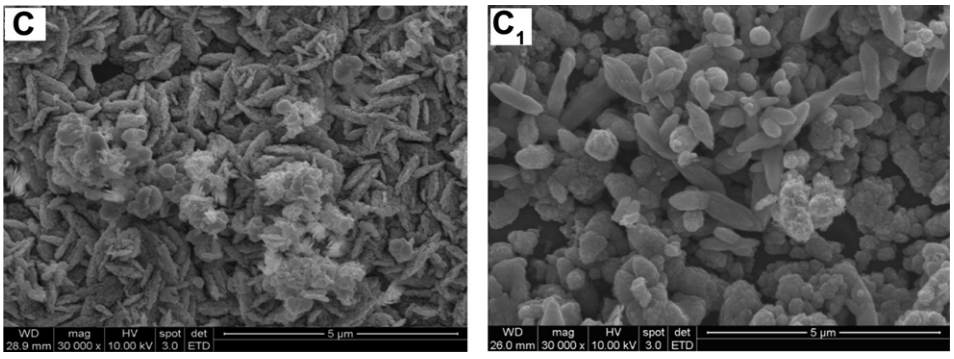


Fig. 4. SEM images of (c) as-Deposited and (c_1) annealed SnO_2 thin films at 30000× magnification.

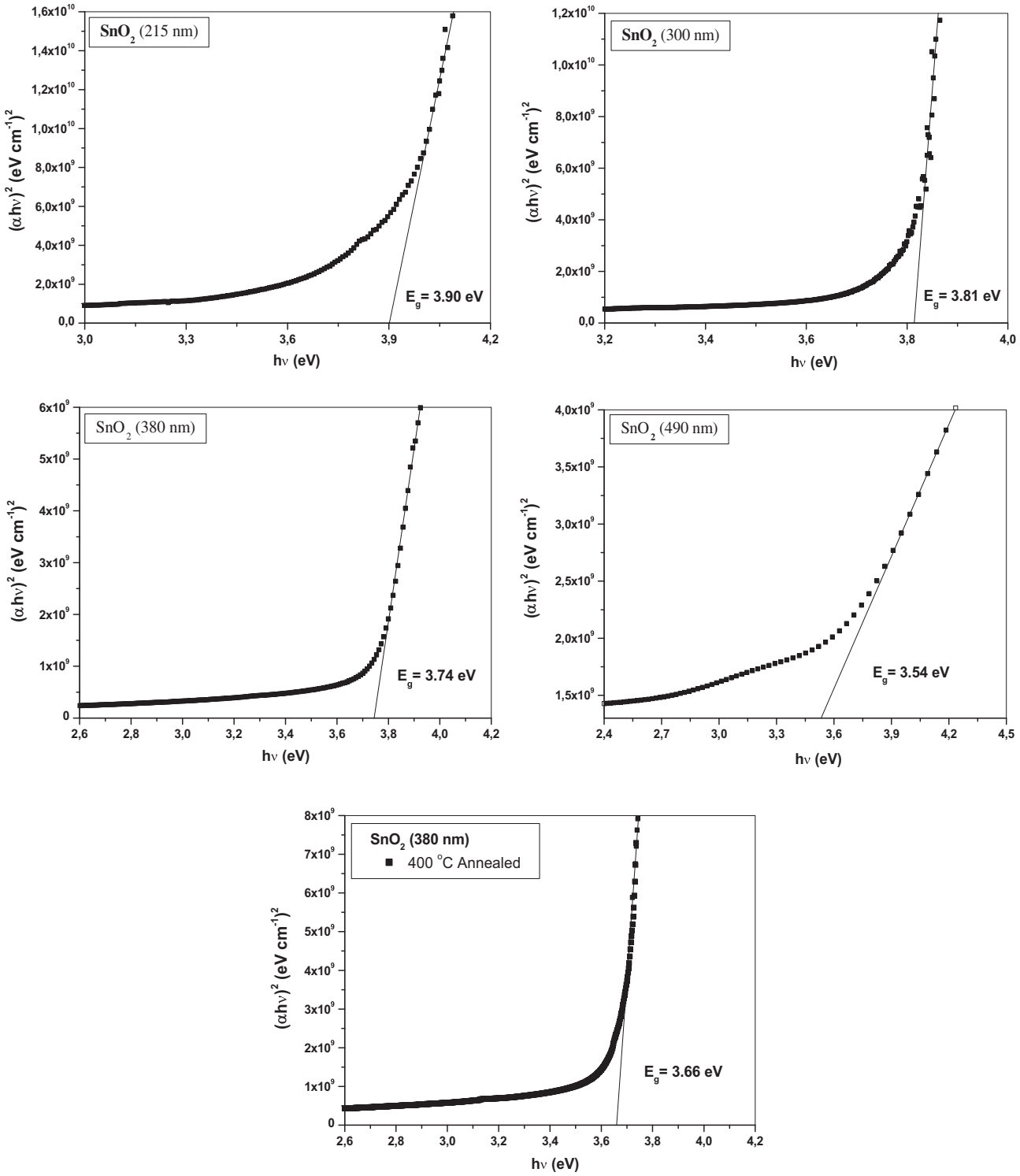


Fig. 5. Plot of $(\alpha h\nu)^2$ versus $h\nu$ for SnO_2 thin films as a function of film thickness and annealed temperature.

was calculated using Moss relation [24,25] which is directly related to the fundamental energy bandgap (E_g),

$$E_g n^4 = k \tag{6}$$

where k is a constant with a value of 108 eV. A different relation between the refractive index and bangap energy is presented by Herve and Vandamme in the following for [26,27],

$$n = \sqrt{1 + \left(\frac{A}{E_g + B}\right)^2} \tag{7}$$

where A and B are numerical constants with values of 13.6 and 3.4 eV, respectively. The changing of refractive index (n) with film thickness and annealing temperature is shown in Table 2 for these two models. As is seen from the Table 2, the refractive index values

Table 2
The bandgap (E_g), refractive index (n), optical static dielectric constant (ε_o) and optical high frequency dielectric constant (ε_∞) values of SnO_2 thin films as a function of film thickness and annealed temperature.

SnO_2	E_g (eV)	ε_o	Moss relation		Herve &Vandamme	
			n	ε_∞	n	ε_∞
215 nm	3.90	6.51	2.29	5.24	2.11	4.45
300 nm	3.81	6.78	2.30	5.29	2.13	4.53
380 nm	3.74	7.00	2.32	5.38	2.15	4.62
490 nm	3.54	7.62	2.35	5.52	2.20	4.84
400 °C (380 nm)	3.66	7.24	2.33	5.42	2.17	4.70

increased from 2.11 to 2.35 with increasing film thickness. However, the rate of increase seems to be dependent on the used models. Since n is strongly connected with band gap energy, it can be concluded that the smaller band gap energy material has a larger value of the n.

The dielectric behavior of solids is important for several electron-device properties. Both static and high frequency dielectric constants were evaluated for all the films. The high frequency dielectric constant (ε_∞) was calculated from the following relation [25],

$$\varepsilon_\infty = n^2 \tag{8}$$

where n is refractive index. The static dielectric constant (ε_o) of the films was calculated using a relation expressing the energy band gap dependence of ε_o for semiconductors compounds in the following form [26,28],

$$\varepsilon_o = 18.52 - 3.08E_g \tag{9}$$

For different film thicknesses and annealing temperature (400 °C), the calculated n, ε_∞ and ε_o values of the SnO_2 films were presented in Table 2. All of these results are in agreement with relevant literature [3,12,29].

3.4. Electrical characterization

The measurements of electrical conductivity of the SnO_2 thin films were carried out in the temperature range 300–500 K using the two-point-probe method under dark media. The plots of inverse absolute temperature versus lnσ are shown in Figs. 6 and 7. As is seen in Figs. 6 and 7 and Table 3, the electrical conductivity values increased with increasing temperature and film thickness.

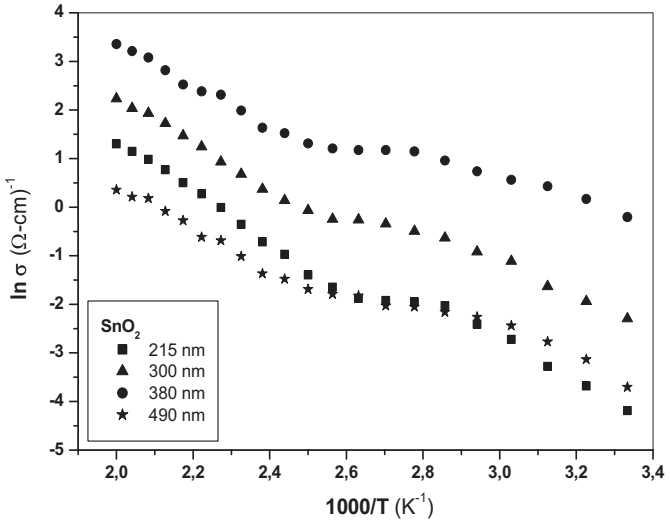


Fig. 6. Plots of ln σ versus (1000/T) for SnO_2 thin films as a function of film thickness.

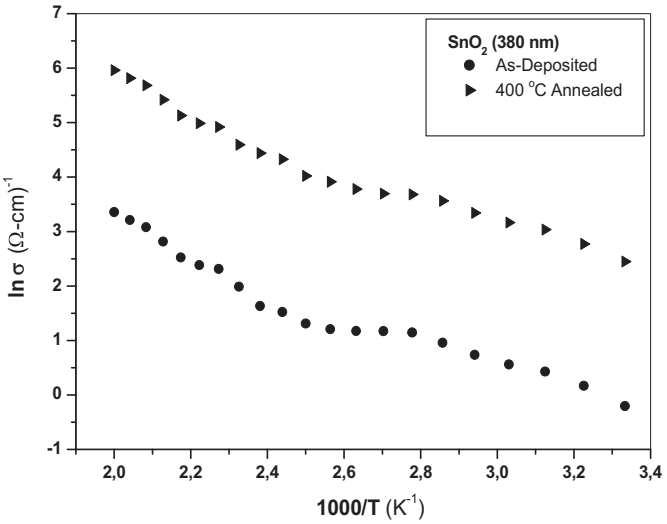


Fig. 7. Plots of ln σ versus (1000/T) for SnO_2 thin films as a function of annealed temperature.

Table 3
The electrical conductivity (σ) and activation energy (E_a) values of SnO_2 thin films.

SnO_2	σ (Ω-cm)$^{-1}$		E_a (eV)	
	300 K	500 K	LR	HR
215 nm	0.015	3.669	0.38	0.45
300 nm	0.100	9.324	0.28	0.41
380 nm	0.815	28.689	0.20	0.37
490 nm	0.024	1.428	0.32	0.39
400 °C (380 nm)	11.588	387.810	0.18	0.31

LR: low temperature region and HR: high temperature region.

Conductivity increased from 0.015 (Ω-cm)$^{-1}$ for 215 nm to 0.815 (Ω-cm)$^{-1}$ for 380 nm film thickness. Also, conductivity increased significantly from 0.815 (Ω-cm)$^{-1}$ to 11.588 (Ω-cm)$^{-1}$ with annealing temperature (Fig. 7 and Table 3). The increasing in conductivity with increasing film thickness and annealing effect can be attributed to the improvement of the crystallization, morphological changes of the films and removal of tin hydroxide which may resist the electrical conduction between grains. However, conductivity decreased to 0.024 (Ω-cm)$^{-1}$ for 490 nm film thickness (Fig. 6 and Table 3). This decreasing in conductivity may be attributed to the deterioration of crystallinity, decrease in oxygen vacancies and charge carrier density. As is seen in Figs. 6 and 7 and Table 3, the activation energies were calculated for two linear regions. The activation energies of the films were found to be in the range of 0.38–0.20 eV at low temperature range and 0.45–0.37 eV at high temperature range with increasing film thickness (in Table 3). These results are in agreement with literature, XRD and SEM results [2–4,6,9,24,30].

4. Conclusions

There are many growth methods for thin film growths. But according to the other methods, SILAR method is simple, fast, sensitive and cheap to prepare thin films. Hence, SnO_2 thin films were synthesized on glass substrates by using simple and economical SILAR method at room temperature. The influence of film thickness on the structural, morphological, optical and electrical properties of SnO_2 thin films was extensively studied. The XRD and SEM studies showed that SnO_2 thin films had a polycrystalline structure with tetragonal, the crystalline and surface properties of these thin films were improved with increasing film thickness and annealing effect. The crystallinity and surface of films began to break down after

380 nm film thickness. The band gap values decreased from 3.90 to 3.54 eV and the refractive index (n) of the films increased from 2.11 to 2.35 with increasing film thickness. The film thickness effect on static and high frequency dielectric constants (ε_0, ε_∞) was also studied. The conductivity values increased significantly with increasing film thickness and annealing temperature. Hence, SnO_2 and its relative low cost, make it preferable in some applications requiring a conducting layer on glass. Consequently, it can be indicated that the film thickness and annealing temperature play an important role on the characteristic parameters of the films and SILAR is a suitable method for depositing SnO_2 thin films.

Acknowledgement

We would like to acknowledge the financial support given by the Erzincan University Research Foundation, Project No: 10.01.07.

References

[1] R.K. Gupta, K. Ghosh, R. Patel, S.R. Mishra, P.K. Kahol, Mater. Lett. 62 (2008) 3373–3375.
[2] M. Ali Yıldırım, Aytunç Ateş, Opt. Commun. 283 (2010) 1370–1377.
[3] A.F. Khan, M. Mehmood, M. Aslam, M. Ashraf, Appl. Surf. Sci. 256 (2010) 2252–2258.
[4] T. Ohgaki, R. Matsuoka, K. Watanable, K. Matsumoto, Y. Adachi, I. Sakaguchi, S. Hishita, N. Ohashi, H. Haneda, Sens. Actuators B 150 (2010) 99–104.
[5] N.G. Deshpande, J.C. Vyas, R. Sharma, Thin Solid Films 516 (2008) 8587–8593.
[6] D.P. Joseph, P. Renugambal, M. Saravanan, S.P. Raja, C. Venkateswaran, Thin Solid Films 517 (2009) 6129–6136.
[7] G. Korotcenkov, B.K. Cho, Sens. Actuators B 142 (2009) 321–330.
[8] D. Miao, Q. Zhao, S. Wu, Z. Wang, X. Zhang, X. Zhao, J. Non-Crystall. Solids 356 (2010) 2557–2561.
[9] E. Elangovan, M.P. Singh, K. Ramamurthi, Mater. Sci. Eng. B 113 (2004) 143–148.
[10] A.A. Yadav, E.U. Masumdar, A.V. Moholkar, M.N. Spallart, K.Y. Rajpure, C.H. Bhosale, J. Alloys Compd. 488 (2009) 350–355.
[11] A.F. Khan, M. Mehmood, A.M. Rana, M.T. Bhatti, Appl. Surf. Sci. 255 (2009) 8562.
[12] S. Goldsmith, E. Çetinörgü, R.L. Boxman, Thin Solid Films 517 (2009) 5146–5150.
[13] G. Brauer, J. Szczyrbowski, G. Teshner, Surf. Coat. Technol. 94 (95) (1997) 658.
[14] V.N. Zhitomirsky, T. David, R.L. Boxman, S. Goldsmith, A. Verdyan, Y.M. Soifer, L. Rapoport, Thin Solid Films 492 (2005) 187–194.
[15] J.R. Brown, P.W. Haycock, L.M. Smith, A.C. Jones, E.W. Williams, Sens. Actuators B 63 (2000) 109.
[16] M. Ali Yıldırım, Aytunç Ateş, Sens. Actuators A 155 (2009) 272–277.
[17] C.S. Barrett, T.B. Massalski, Structure of Metals, Pergamon, Oxford, 1980, p. 204.
[18] W.D. Callister, Materials Science and Engineering–an Introduction, John Wiley and Sons, New York, 1997.
[19] M. Ashraf, S.M.J. Akhtar, A.F. Khan, Z. Ali, A. Qayyum, J. Alloys Compd. 509 (2011) 2414–2419.
[20] E. Rosencher, B. Vinter, Optoelectronics, Cambridge University Press,, 2002, p. 304.
[21] V. Geraldo, L.V.A. Scalvi, E.A. Morais, C.V. Santilli, P.B. Miranda, T.J. Pereira, J. Eur. Ceram. Soc. 25 (2005) 2825–2828.
[22] Yin Tang, Synthesıs and Characterızatıon of Tın Oxıde for Thın Fılm Gas Sensor Applıcatıons (2004).
[23] H.M. Pathan, B.R. Sankapal, J.D. Desai, C.D. Lokhande, Mater. Chem. Phys. 78 (2002) 11–14.
[24] Y. Akaltun, M.A. Yıldırım, A. Ateş, M. Yıldırım, Opt. Commun. 284 (2011) 2307–2311.
[25] L. Hannachi, N. Bouarissa, Physica B 404 (2009) 3650–3654.
[26] F. Mezrag, W.K. Mohamed, N. Bouarissa, Physica B 405 (2010) 2272–2276.
[27] P. Herve, L.K.J. Vandamme, Infrared Phys. Technol. 35 (1994) 609.
[28] S. Adachi, Properties of Group IV, III-V and II-VI Semiconductors, Wiley, Chishester, 2005.
[29] E. Çetinörgü, S. Goldsmith, R.L. Boxman, J. Crystal Growth 299 (2007) 259–267.
[30] J. Lee, Thin Solid Films 516 (2008) 1386–1390.